

# One-Way Multiple Beam Splitter Designed by Quantum-like Shortcut-to-Adiabatic Passage

Jiahui Zhang<sup>1,\*</sup>

<sup>1</sup>*School of Physics, East China University of Science and Technology, Shanghai 200237, China*

Based on the quantum mechanical “Shortcut-to-Adiabatic passage” (STAP), a novel design for the efficient and robust multiple beam splitter is presented in this paper. This multiple beam splitter consists of one input and  $N$  output waveguide channels, which are connected via a mediator waveguide (WG). In contrast to previously suggested adiabatic multiple beam splitter based on an analog of stimulated Raman adiabatic passage (STIRAP) from quantum optics [A. A. Langelov and N. V. Vitanov, *Phys. Rev. A* **85**, 055803 (2012)], the propagation of light wave in the current device can mimic the quantum evolution controlled with “STAP” by meticulously modifying inter-WG coupling strengths. To implement “STAP” but without additional couplings, this  $(N + 2)$ -WG system is first reduced to a controllable 3-WGs counterpart by “Morris-Shore” (MS) transformation. Consequently, this system can be directly compatible with all possible “STAP” methods. The results show that this novel design can achieve arbitrary ratio of high-fidelity multiple beam splitting and can significantly shorten the length of the device, which expands the application of “STAP” in classical system and provides a direct visualization in space of typical ultrafast phenomena in time. More uniquely, this multiple beam splitter exhibits a one-way energy transport behavior. These may have profound impacts on exploring quantum technologies for promoting advanced optical devices.

## I. INTRODUCTION

Adiabatic passage (AP), initially proposed to achieve efficient and robust population transfer between quantum states, has been widely explored and applied in quantum optics and integrated optics [1–14]. When carrying out classical analogs of the AP [15], the well-known STIRAP and its variants were most investigated due to their advantages of being robust, simple, and efficient [16–20]. Examples includes analogies of STIRAP in a three-WG directional coupler [21, 22], fractional-STIRAP [23], multistate-STIRAP [24–28] and STIRAP via the continuum [29, 30]. Among them, the design of beam splitter, which splits incident wave into multiple parts with the same or different intensities, is quite demanding, it has potential applications in optical circuits and communications [13, 31–39]. While the  $1 \times 2$  optical splitters are used routinely [40], the rapidly growing need for space-division multiplexing (SDM) in optical transmission [41], computing [42] and sensing networks [43] translates into the need for multiport splitters [44–46].

Generally adiabatic devices profit from similar properties as AP but suffer from a fundamental limitation in terms of speed, either in time (such as atomic systems), or in space (such as photonic systems) [16]. Specifically, adiabatic coupling requires a long spatial variation of device to satisfy the adiabatic condition [47]. This will cost more space and resources and reduce device density, which is a major disadvantage in integrated optics based on densely integrated optical WGs. To overcome this problem, a range of methods referred as “Shortcut-to-Adiabatic passage” (STAP) [48, 49], which was initially proposed to accelerate adiabatic quantum-state transfer

[40, 50–60], has recently been applied to design WG devices [61–73]. It presents significant advantages with respect to conventional STIRAP-like schemes, such as relaxing the the demands of the exact evolution. Integrated optics waveguide platform enabled by the advanced micro/nano fabrication technology provides an ideal platform to realize the device geometries designed by various “STAP” protocol [74]. A recent review on the applications of “STAP” methods in optical WGs can be found in Ref. [75]. Despite numerous achievements in the field of optics, the application of “STAP” in multiple beam splitter has not been widely reported to date, especially its ability to obtain arbitrary beam splitting and achieve one-way energy transport.

In this paper, by performing an analog of the quantum-mechanical “STAP” in classic optical system, a theoretical method for achieving efficient and robust multiple beam splitting is proposed. This optical multiple beam splitter consists of one input and  $N$  output WG channels, which are connected via a mediator WG. With the modified inter-WG coupling strengths, the behaviors of beam splitting with arbitrary ratio as well as complete energy transfer are capable of realizing in the same coupler by selecting different input ports. Furthermore, the results prove that this coupled-WG system can reduce the length of device and exhibit a one-way energy transport behavior. These properties make it possible to design some interesting WG devices.

## II. MODEL AND METHOD

The quantum systematic counterpart of the waveguide structure considered in this paper is shown in Fig. 1(a), in which the initial state  $|i\rangle$  is coupled to the excited state  $|m\rangle$  with a pump pulse  $\Omega_P(t)$ , and the other  $N$  ground states  $|1\rangle, |2\rangle, \dots, |n\rangle$  are also coupled to the excited state

\* [y10220159@mail.ecust.edu.cn](mailto:y10220159@mail.ecust.edu.cn)

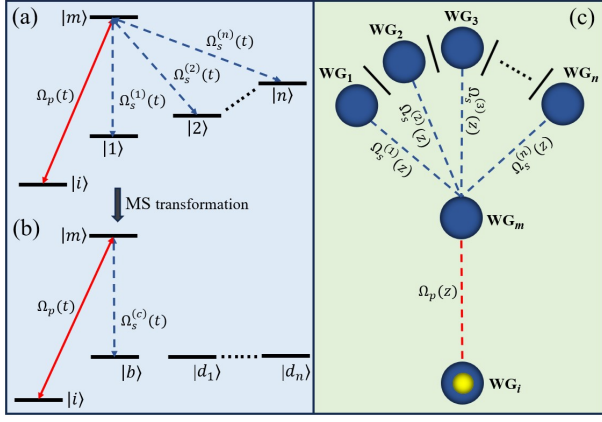


FIG. 1. (Color online) (a) Linkage pattern of the  $N$ -pod system [76]; (b) The effective 3-level quantum counterpart after the MS transformation; (c) Cross section of a possible waveguide arrangement of the multiple beam splitter. The dashed lines depict the couplings between the WGs, which are changed by changing the distance between the WGs [44].

with a battery of Stokes pulses  $[\Omega_S^{(1)}(t), \Omega_S^{(2)}(t) \dots \Omega_S^{(n)}(t)]$ . The evolution can be described by the time-dependent Schrödinger equation:

$$i\hbar \frac{d}{dt} \psi(t) = H(t) \psi(t), \quad (1)$$

where  $\psi(t) = [\psi_i(t), \psi_m(z), \psi_1(z), \dots, \psi_n(z)]^T$  with  $\psi_k(t)$  being the probability amplitude of the state  $|k\rangle$  ( $k = i, m, 1, \dots, n$ ). Under the rotating-wave approximation, the Hamiltonian  $H(t)$  is written as

$$H(t) = \begin{bmatrix} 0 & \Omega_P(t) & 0 & \dots & 0 \\ \Omega_P(t) & 0 & \Omega_S^{(1)}(t) & \dots & \Omega_S^{(n)}(t) \\ 0 & \Omega_S^{(1)}(t) & 0 & \dots & 0 \\ \vdots & \vdots & \vdots & \ddots & \vdots \\ 0 & \Omega_S^{(n)}(t) & 0 & 0 & 0 \end{bmatrix}. \quad (2)$$

Based on the MS transformation [77, 78], one can simplify the analysis by reducing the dynamics of this  $(N+2)$ -level quantum system into controllable three-level one, as illustrated in Fig. 1(b). The transformed Hamiltonian under MS basis  $\{|i\rangle, |m\rangle, |b\rangle\}$  can be read as follows:

$$H_T(t) = \begin{bmatrix} 0 & \Omega_P(t) & 0 \\ \Omega_P(t) & 0 & \Omega_S^{(c)}(t) \\ 0 & \Omega_S^{(c)}(t) & 0 \end{bmatrix}. \quad (3)$$

where a bright superposition  $|b\rangle$  is coupled to  $|m\rangle$  with a coupling which is the root-mean-square (rms) of the initial couplings,

$$\Omega_S^{(c)}(t) = \sqrt{\sum_{j=1}^n [\Omega_S^{(j)}(t)]^2}, \quad (4)$$

The bright superposition has the vector form

$$|b\rangle = \frac{[0, 0, \Omega_S^{(1)}(t), \Omega_S^{(2)}(t), \dots, \Omega_S^{(N)}(t)]^T}{\Omega_S^{(c)}(t)}. \quad (5)$$

Diagonalizing Hamiltonian (3), one can obtain three eigenvectors

$$|\Phi_0(t)\rangle = \begin{bmatrix} \cos \alpha(t) \\ 0 \\ -\sin \alpha(t) \end{bmatrix}, |\Phi_{\pm}(t)\rangle = \begin{bmatrix} \sin \alpha(t) \\ \pm 1 \\ \cos \alpha(t) \end{bmatrix} / \sqrt{2}. \quad (6)$$

where the mixing angle  $\tan \alpha(t) = \Omega_S^{(c)}(t) / \Omega_P(t)$ . In principle, if adiabatic conditions are satisfied, a perfect population transfer from  $|i\rangle$  to superposition  $|b\rangle$  can be achieved via a STIRAP-like process [16]. However, a perfect quantum-state transfer needs to satisfy the adiabatic criterion. This means it requires a very long evolution time, analogous to requiring a long spatial variation of device. Therefore, it is necessary to speed-up the adiabatic procedure towards the perfect final outcome. Although a solution for implementing “STAP” in  $N$ -pod system has recently been proposed [79], the proposal requires additional couplings among initial state  $|i\rangle$  and the final ground states  $|1\rangle, |2\rangle, \dots, |n\rangle$ , which is generally difficult or even impossible for practical implementations. Particularly, the existence of non-adjacent or imaginary coupling coefficients makes the proposal unrealistic in the current multiple beam splitter. To implement “STAP” but without additional couplings, one can introduce a pair of counter-adiabatic pulses into  $\Omega_P(t)$  and  $\Omega_S^{(c)}(t)$ , to find a pair of modified coupling pulses  $\tilde{\Omega}_P(t)$  and  $\tilde{\Omega}_S^{(c)}(t)$ . In principle, such a pair of modified pulses can be obtained by several three-level “STAP” methods [54, 80–84]. The form of the modified Hamiltonian can thus be written

$$\tilde{H}_T(t) = \begin{bmatrix} 0 & \tilde{\Omega}_P(t) & 0 \\ \tilde{\Omega}_P(t) & 0 & \tilde{\Omega}_S^{(c)}(t) \\ 0 & \tilde{\Omega}_S^{(c)}(t) & 0 \end{bmatrix}. \quad (7)$$

Among the methods mentioned above, let us use the “chosen paths” method [83, 85] as an example to demonstrate our treatment of this waveguide system. The “chosen paths” method supports the following dressed states [85]

$$|\Phi'_0(t)\rangle = \begin{bmatrix} \cos \mu(t) \cos \theta(t) \\ i \sin \mu(t) \\ \cos \mu(t) \sin \theta(t) \end{bmatrix}, \quad (8)$$

$$|\Phi'_{\pm}(t)\rangle = \begin{bmatrix} \sin \theta(t) \mp i \sin \mu(t) \cos \theta(t) \\ \mp \cos \mu(t) \\ -\cos \theta(t) \mp i \sin \mu(t) \sin \theta(t) \end{bmatrix} / \sqrt{2}. \quad (9)$$

It is convenient to move  $\tilde{H}_T(t)$  to the frame with the time-independent chosen paths being basis by the unitary

operator  $U_0 = \sum_{\xi=\pm,0} |\Phi'_\xi(t)\rangle\langle\Phi'_\xi(t)|$ . Hamiltonian (7) in new frame becomes

$$\begin{aligned}\tilde{H}'_T(t) &= U_0(t)\tilde{H}_T(t)U_0^\dagger(t) - iU_0(t)\dot{U}_0^\dagger(t) \\ &= \Lambda(t)(|\Phi'_+(t)\rangle\langle\Phi'_+(t)| - |\Phi'_-(t)\rangle\langle\Phi'_-(t)|) \\ &\quad + [\eta_+(t)|\Phi'_+(t)\rangle\langle\Phi'_0(t)| \\ &\quad + \eta_-(t)|\Phi'_-(t)\rangle\langle\Phi'_0(t)| + H.c.].\end{aligned}\quad (10)$$

Obviously, only  $\eta_\pm(t) = 0$  ensures the elimination of the interactions of  $|\Phi'_0(t)\rangle$  and  $|\Phi'_\pm(t)\rangle$ . Accordingly, one can easily derive that

$$\tilde{\Omega}_P(t) = -\dot{\theta}(t)\sin\theta(t)\cot\mu(t) - \dot{\mu}(t)\cos\theta(t), \quad (11)$$

$$\tilde{\Omega}_S^{(c)}(t) = \dot{\theta}(t)\cos\theta(t)\cot\mu(t) - \dot{\mu}(t)\sin\theta(t). \quad (12)$$

The state function of the system can also be mapped into the dressed-state space by [86]

$$|\Phi'(t)\rangle = \sum_{\xi=0,\pm} \tilde{A}_\xi(t)|\Phi'_\xi(t)\rangle, \quad (13)$$

where  $\tilde{A}_\xi(t) = a_\xi(t_0)\exp[-i\int_{t_0}^t \varepsilon_\xi(t')dt']$  with  $a_\xi(t_0)$  being determined by the initial state  $|\Phi'(t_0)\rangle$  and  $\varepsilon_\xi(t) = \langle\Phi'_\xi(t)|H_M(t)|\Phi'_\xi(t)\rangle$ . For a given condition of  $a_0(t_0) = 1$  and  $a_+(t_0) = a_-(t_0) = 0$ , the state function follows the evolution of  $|\Phi'_0(t)\rangle$ . Thus, a perfect quantum state transfer from  $|i\rangle$  to  $|b\rangle$  can be achieved when  $\mu(t)$  and  $\theta(t)$  satisfy  $\mu(t_0) = \mu(t_f) = 0, \theta(t_0) = 0, \theta(t_f) = \pi/2$ . For another given condition of  $a_0(t_0) = 0$  and  $a_+(t_0) = a_-(t_0) = 1/\sqrt{2}$ , the state function follows the evolution of superposition states of  $|\Phi'_\pm(t)\rangle$ . Given by Eq. (13), the state transfer from  $|b\rangle$  to  $|m\rangle$  can be realized under the same conditions adopted in the state transfer from  $|i\rangle$  to  $|b\rangle$ . It is quite interesting that population transfer is realized from  $|i\rangle$  to  $|b\rangle$ , while from  $|b\rangle$  to  $|m\rangle$  under the same condition, showing an asymmetric transfer behavior in this system.

Now let us go back to the  $(N+2)$ -level quantum system and design the modified pulses by comparing the Hamiltonian (3) and (7). Like Eq. (4), one can impose

$$\tilde{\Omega}_S^{(c)}(t) = \sqrt{\sum_{j=1}^n [\tilde{\Omega}_S^{(j)}(t)]^2}, \quad (14)$$

and calculate inversely the modified pulses as

$$\sum_{j=1}^n [\tilde{\Omega}_S^{(j)}(t)]^2 = (\tilde{\Omega}_S^{(c)})^2(t), \quad (15)$$

which leads to a modified Hamiltonian with the same form as Hamiltonian (2)

$$\tilde{H}(t) = \begin{bmatrix} 0 & \tilde{\Omega}_P(t) & 0 & \cdots & 0 \\ \tilde{\Omega}_P(t) & 0 & \tilde{\Omega}_S^{(1)}(t) & \cdots & \tilde{\Omega}_S^{(n)}(t) \\ 0 & \tilde{\Omega}_S^{(1)}(t) & 0 & \cdots & 0 \\ \vdots & \vdots & \vdots & \ddots & \vdots \\ 0 & \tilde{\Omega}_S^{(n)}(t) & 0 & 0 & 0 \end{bmatrix}. \quad (16)$$

This Hamiltonian can describe other physical systems apart from the quantum system shown in Fig. 1(a). For example it represents in the paraxial approximation and substituting time by a longitudinal coordinate  $(N+2)$  coupled WGs [44, 87], where the couplings be controlled by waveguide separation. In particular  $\tilde{\Omega}_P(t \rightarrow z)$  and  $\tilde{\Omega}_S^{(n)}(t \rightarrow z)$  may be manipulated to split the input wave into two output channels [36, 88, 89] or multiple output channels [44]. At the same time, due to the analogies between quantum mechanics and wave optics, the beam splitting allows us to visualize the evolution of the particle wave function in a tripod system [90, 91] or a multipod system [92, 93] at a macroscopic level.

By mapping the above results into spatial dimension [87], as shown in Fig. 1(c), our analogy in an optical system is proposed by a  $(N+2)$ -WG coupler. Fig. 1(c) shows a cross section of the possible geometry of this device, the structure is similar to that reported in Refs. [36, 44, 88, 89], consisting of one input WG<sub>i</sub>, one mediator WG<sub>m</sub>, and finite number of  $N$  output WG<sub>n</sub>. The dashed lines in the diagram depict the couplings between the WGs, which depend strongly on the distance between the WGs due to the evanescent-wave nature of the waveguide couplings. Following most of the earlier case studies [36, 44, 88, 89], here we also consider only coupling between nearest neighbors (nearest-neighbor approximation). The output WGs should be isolated from each other and should only be coupled to the mediator WG<sub>m</sub>, thus optical isolators are needed to avoid the unwanted coupling actions between the WGs [44, 89]. Assisted by the agreement in the form between Schrödinger equation in quantum mechanics and the coupled-mode equation of classical waves [87, 94], the propagation of the optical fields in waveguide structure can be described by the modified coupling matrix shown below

$$\tilde{H}(z) = \begin{bmatrix} 0 & \tilde{\Omega}_P(z) & 0 & \cdots & 0 \\ \tilde{\Omega}_P(z) & 0 & \tilde{\Omega}_S^{(1)}(z) & \cdots & \tilde{\Omega}_S^{(n)}(z) \\ 0 & \tilde{\Omega}_S^{(1)}(z) & 0 & \cdots & 0 \\ \vdots & \vdots & \vdots & \ddots & \vdots \\ 0 & \tilde{\Omega}_S^{(n)}(z) & 0 & 0 & 0 \end{bmatrix}. \quad (17)$$

The modified coupling strength between WG<sub>i</sub> and WG<sub>m</sub> is  $\tilde{\Omega}_P(z)$  and the one between WG<sub>m</sub> and WG<sub>n</sub> are  $\tilde{\Omega}_S^{(n)}(z)$  ( $n = 1, 2, \dots, N$ ), which play the roles of Rabi frequencies for pump and Stokes pulses in quantum physics, respectively. They can be expressed as

$$\tilde{\Omega}_P(z) = -\dot{\theta}(z)\sin\theta(z)\cot\mu(z) - \dot{\mu}(z)\cos\theta(z), \quad (18)$$

$$\tilde{\Omega}_S^{(c)}(z) = \dot{\theta}(z)\cos\theta(z)\cot\mu(z) - \dot{\mu}(z)\sin\theta(z), \quad (19)$$

and

$$\sum_{j=1}^n [\tilde{\Omega}_S^{(j)}(z)]^2 = (\tilde{\Omega}_S^{(c)})^2(z), \quad (20)$$

where the overdot denotes the  $z$ -derivative. In typical implementations where the coupling strengths can be modulated by changing the distance between the WGs. The evolution of the wave amplitudes in this  $(N+2)$ -WG optical coupler can be described by the following coupled mode equation [87],

$$i \frac{d}{dz} A(z) = \tilde{H}(z) A(z), \quad (21)$$

where  $A = [a_i(z), a_m(z), a_1(z), \dots, a_n(z)]^T$ ,  $a_k(z)$  ( $k = i, m, 1, \dots, n$ ) is the light amplitude in the  $k$ th waveguide and the dimensionless light intensity is  $I_k = |a_k(z)|^2$ .

To mimic the behavior of the quantum system described above, the mixing angle  $\mu$  and  $\theta$  should satisfy:

$$\mu(z_0) = \mu(z_f) = 0, \quad (22)$$

$$\theta(z_0) = 0, \theta(z_f) = \pi/2. \quad (23)$$

To meet these conditions,  $\mu$  and  $\theta$  can be set as

$$\theta(z) = \frac{\pi z}{2z_f} - \frac{1}{3} \sin\left(\frac{2\pi z}{z_f}\right) + \frac{1}{24} \sin\left(\frac{4\pi z}{z_f}\right), \quad (24)$$

$$\mu(z) = \frac{\zeta}{2} \left[ 1 - \cos\left(\frac{2\pi z}{z_f}\right) \right]. \quad (25)$$

In principle, if light wave is incident of  $WG_i$ , similar to Eq. (8), it follows:

$$|\Phi'_0(z)\rangle = \begin{bmatrix} \cos \mu(z) \cos \theta(z) \\ i \sin \mu(z) \\ \cos \mu(z) \sin \theta(z) \end{bmatrix}, \quad (26)$$

the output port is expected to be  $WG_n$ , the power distribution of each output port can be customized arbitrarily by utilizing respective space-varying coupling  $\tilde{\Omega}_S^{(n)}(z)$ ; if light waves are incident from  $WG_n$  ( $n = 1, 2, \dots, N$ ) simultaneously, similar to Eq. (9), it follows:

$$|\Phi'_\pm(z)\rangle = \begin{bmatrix} \sin \theta(z) \mp i \sin \mu(z) \cos \theta(z) \\ \mp \cos \mu(z) \\ -\cos \theta(z) \mp i \sin \mu(z) \sin \theta(z) \end{bmatrix} / \sqrt{2} \quad (27)$$

the output port is expected to be  $WG_m$ .

To better describe the geometry of the device, let us analyze it in seven stages with  $N = 3$  as an example, as shown in Fig. 2. It can be clearly seen from the figure that (1) when  $z \in (0, 0.162)$ ,  $\Omega_P(z)$  coupling dominates over the  $\tilde{\Omega}_S^{(c)}(z)$  couplings, as shown in the pink area; (2) when  $z = 0.162$ ,  $WG_i$  and  $WG_n$  are equally coupled to  $WG_m$ , as indicated by the location marked by the black circle; (3) when  $z \in (0.162, 0.412)$ ,  $\tilde{\Omega}_S^{(c)}(z)$  couplings dominate over the  $\Omega_P(z)$  couplings, as shown in the yellow area; (4) when  $z = 0.412$ ,  $WG_i$  and  $WG_n$  are equally coupled to  $WG_m$ , as indicated by the location marked by the red circle; (5) when  $z \in (0.412, 0.946)$ ,  $\Omega_P(z)$  coupling dominates over the  $\tilde{\Omega}_S^{(c)}(z)$  couplings, as shown in the grey area; (6) when  $z = 0.946$ ,  $WG_i$  and  $WG_n$  are equally coupled to  $WG_m$ , as indicated by the location marked by the orange circle; (7) when  $z \in (0.946, 1)$ ,  $\tilde{\Omega}_S^{(c)}(z)$  couplings dominate over the  $\Omega_P(z)$  couplings, as shown in the blue area.

### III. RESULTS

Below, let us still limit the model to  $N = 3$  for an explicit demonstration, but the conclusions remain valid in the general case of any  $N$ . For simplicity, the couplings among  $WG_m$  and  $WG_n$  ( $n = 1, 2, 3$ ) are assumed to share the same  $z$ -dependence but they may have in general different magnitudes, i.e.,  $\Omega_S^{(1)}(z) : \Omega_S^{(2)}(z) : \Omega_S^{(3)}(z) = \eta_1 : \eta_2 : \eta_3$ . In the absence of losses the conservation law  $I_i + I_m + \sum_{j=1}^n I_j = 1$  is applied during propagation, like the total population in a coherently driven quantum system. The post-coupling power distribution along each WG can be obtained by solving the coupled mode equation (21) with the coupling matrix (17).

The top frame of Fig. 3 show the well-tailored inter-WG coupling strengths as a function of  $z$ , which are used for equal multiple beam splitting. The blue dash, green dot and red solid lines in Fig. 3(c) illustrate the simulated light intensity distributions along  $WG_i$ ,  $WG_m$ ,  $WG_n$  ( $n = 1, 2, 3$ ), respectively, it can be observed that the light wave input from  $WG_i$  can be equally split to  $WG_1$ ,  $WG_2$  and  $WG_3$  with  $z = 100mm$ . During the propagation, the mediator  $WG_m$  carries a little transient light, which will undoubtedly reduce transmission efficiency. Fortunately, due to the unique property of the “STAP”, one can reproduce the the same perfect efficiencies of multiple beam splitter via a shorter length, as illustrated in Fig. 3(d). Clearly, the device length is reduced to  $1mm$  in this numerical example, corresponding to a significant reduction in device length as compared to  $100mm$ . This is essential for the miniaturization of the device and the reduction of losses during transmission. Another interesting feature is that the multiple beam splitter designed by “STAP” can present a one-way energy transport behavior, that is, if light is incident  $WG_n$  ( $n = 1, 2, 3$ ) simultaneously, a complete energy transfer to  $WG_m$  instead of getting transferred back to  $WG_i$  can be achieved, as shown in Fig. 3(e) and 3(f), which provides additional control over the distribution of light in the WGs. The above asymmetric behavior of energy transfer can be explained by two different evolu-

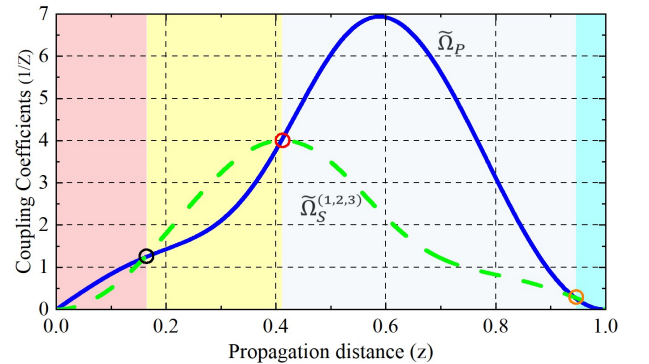


FIG. 2. (Color online) Coupling coefficients as a function of  $z$ . Parameter used:  $\zeta = 0.145\pi$ .



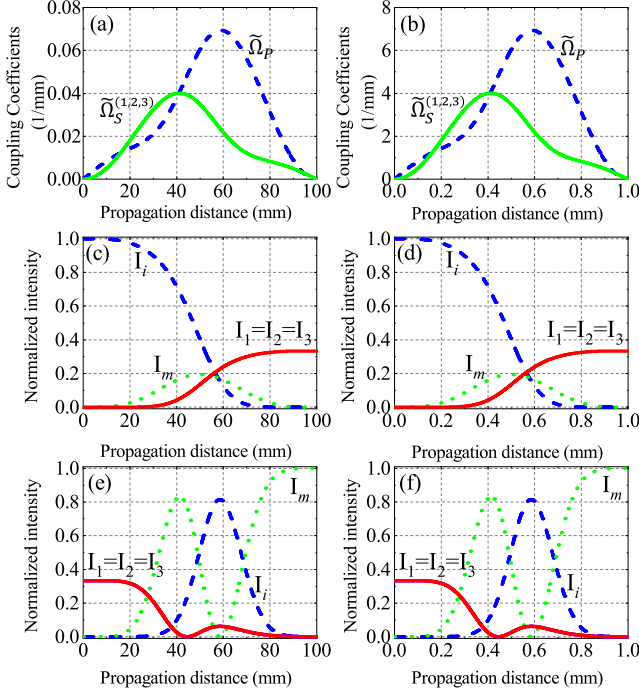


FIG. 3. (Color online) The equal multiple beam splitter designed by “STAP”. Top frame: coupling strengths as a function of  $z$ ; Middle frame: 1 : 1 : 1 beam splitting for  $\eta_1 = \eta_2 = \eta_3$ ; Bottom frame: one-way optical energy transfer. Left column:  $z \in [0, 100]mm$ ; Right column:  $z \in [0, 1]mm$ . Parameter used:  $\varsigma = 0.145\pi$ .

tion processes [89]. For the left port of  $WG_i$  incidence, the evolution follows Eq. (26), thus leading to a result of  $[I_i(z_0), 0, 0, 0, 0] \rightarrow [0, 0, \frac{1}{3}I_1(z_f), \frac{1}{3}I_2(z_f), \frac{1}{3}I_3(z_f)]$  under the conditions of (22) and (23). For the left port of  $WG_n$  ( $n = 1, 2, 3$ ) simultaneous incidence, the evolution follows Eq. (27), exhibiting another result of  $[0, 0, \frac{1}{3}I_1(z_0), \frac{1}{3}I_2(z_0), \frac{1}{3}I_3(z_0)] \rightarrow [0, I_m(z_f), 0, 0, 0]$  under the same conditions of (22) and (23). Indeed, the output port for incidence from  $WG_n$  is closely related to the value of  $\varsigma$ , while the output port for incidence from  $WG_i$  is immune to the value of  $\varsigma$ . The detailed explanations are presented in Appendix VI.

To further illustrate the advantages of device designed by “STAP”, now let us compare it with the previously proposed adiabatic device based on an analog of “STIRAP”. As discussed in Sec. II, a perfect adiabatic quantum state transfer from  $|i\rangle$  to  $|b\rangle$  can be achieved by a STIRAP-like process, which can be mapped into space dimension as well. Replacing the spatial variation  $t$  with the temporal variation  $z$ , Eq. (2) can be used to describe the state evolution of this  $(N + 2)$ -WG coupler, this requires the WGs must be arranged in such a manner that the rms coupling  $\tilde{\Omega}_S^{(c)}(z)$  precedes the  $\tilde{\Omega}_P(z)$  coupling but the two must overlap partly, as in “STIRAP” [44]. A popular choice is the coupling coefficients to have the

following Gaussian form [5]

$$\Omega_P(z) = \Omega_0 \exp[-(\frac{z - \tau - z_f/2}{\varsigma})^2], \quad (28)$$

$$\Omega_S^{(c)}(z) = \Omega_0 \exp[-(\frac{z + \tau - z_f/2}{\varsigma})^2], \quad (29)$$

where  $\Omega_0$  is the maximum value of the coupling coefficients,  $\varsigma$  denotes the width of the couplings and  $2\tau$  is the spatial separation between their peaks.

In the contrast between the two, we introduce a strong wave dissipation in  $WG_m$  with a constant damping rate  $\gamma = 0.01\pi$ , which reflects the lossy characteristic of  $WG_m$ . This is mainly based on two considerations: (i) for the current “STAP”-based design, the mediator  $WG_m$  inevitably receives some transient distribution (see Fig. 3); (ii) for devices designed by AP, this problem is still unavoidable because the adiabatic conditions is very hard to reach experimentally [24]. In this case, the coupling matrix in Eqs. (17) and (2) ( $t \rightarrow z$ ) can be changed into a non-Hermitian form [56, 95]. For example, Eq. (17) can be rewritten as

$$\tilde{H}_\gamma(z) = \begin{bmatrix} 0 & \tilde{\Omega}_P(z) & 0 & \cdots & 0 \\ \tilde{\Omega}_P(z) & -i\gamma & \tilde{\Omega}_S^{(1)}(z) & \cdots & \tilde{\Omega}_S^{(n)}(z) \\ 0 & \tilde{\Omega}_S^{(1)}(z) & 0 & \cdots & 0 \\ \vdots & \vdots & \vdots & \ddots & \vdots \\ 0 & \tilde{\Omega}_S^{(n)}(z) & 0 & 0 & 0 \end{bmatrix}. \quad (30)$$

The upper frame of Fig. 4 shows the final light distribution under the “STIRAP” protocol as a function of  $\Omega_0$  and device length. Fig. 4(a) shows the case of the light wave is initially incident from  $WG_i$ , we can easily obtain that the transmission efficiencies are closely related to the coupler length and  $\Omega_0$ . Near-perfect beam splitting from  $WG_i$  to  $WG_n$  ( $n = 1, 2, 3$ ) can be realized only when  $\Omega_0$  is sufficiently large and the device length is long enough (where the adiabatic condition is fully satisfied). Fig. 4(b) shows the final intensity distribution in  $WG_i$  when the light wave is initially incident from  $WG_n$ , the result clearly shows that in most of the parameter space, the light incident from  $WG_n$  ( $n = 1, 2, 3$ ) is transferred to  $WG_i$  rather than localized in  $WG_m$ , indicating that the multiple beam splitter designed by “STIRAP” does not exhibit good one-way energy transport behavior. In contrast, the multiple beam splitter designed by “STAP” presents a number of advantages. The lower frame of Fig. 4 shows the final light distribution against device lengths via “STAP”. Fig. 4(c) corresponds to the case of the light wave is initially incident from  $WG_i$ , from which we can see that in the presence of strong wave dissipation, near-perfect beam splitting from  $WG_i$  to  $WG_n$  ( $n = 1, 2, 3$ ) requires the device length to be as short as possible. This is the exact opposite of the former. On the other hand, if the light wave incident from  $WG_m$  simultaneously, as illustrated in Fig. 4(d), it can be observed that the output wave will be localized in  $WG_m$ , and if the length of the device is very short, the output

wave is almost completely localized in  $WG_m$ , and as the length of the device increases, the light intensity localized in  $WG_m$  will gradually dissipate. Therefore, our device exhibits very good one-way energy transport behavior so long as the time-dependent driving pulse can be fitted well in the spatial dimension.

More interestingly, this multiple beam splitter can achieve arbitrary multiple beam splitting for  $WG_i$  incidence, while no apparent intensity from  $WG_i$  can be obtained for  $WG_n (n = 1, 2, 3)$  simultaneous incidence, as shown in Fig. 5. The corresponding modified inter-WG coupling strengths as a function of  $z$  are shown in the top frame of Fig. 5. Fig. 5(c) and 5(d) illustrate the simulated light intensity distributions with  $z = 100mm$  and  $1mm$ , respectively. It can be observed that the light wave input from  $WG_i$  can be completely transfer to  $WG_1$ ,  $WG_2$  and  $WG_3$  in a ratio of  $3 : 2 : 1$  for  $\eta_1 : \eta_2 : \eta_3 = \sqrt{3} : \sqrt{2} : 1$ , which implies that the results of  $[I_i(z_0), 0, 0, 0, 0] \rightarrow [0, 0, \frac{3}{6}I_1(z_f), \frac{2}{6}I_2(z_f), \frac{1}{6}I_3(z_f)]$  has been realized. On the contrary, if light is incident from  $WG_n (n = 1, 2, 3)$  simultaneously, a complete energy transfer to  $WG_m$  can be realized, this interesting phenomenon of  $[0, 0, \frac{3}{6}I_1(z_0), \frac{2}{6}I_2(z_0), \frac{1}{6}I_3(z_0)] \rightarrow [0, I_m(z_f), 0, 0, 0]$  as shown in Fig. 5(e) and 5(f).

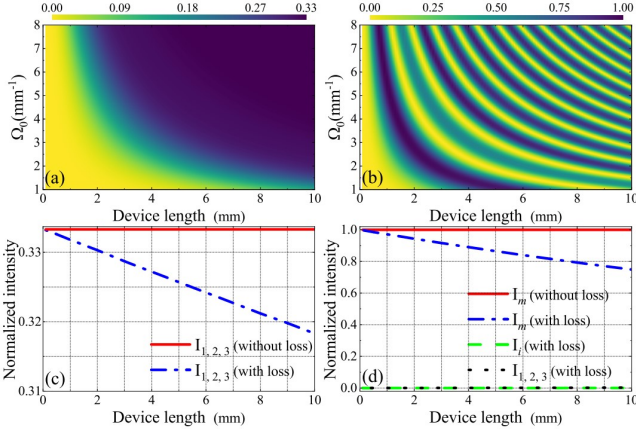


FIG. 4. (Color online) Top frame: the final light distribution under the “STIRAP” protocol as a function of  $\Omega_0$  and device length. (a) and (b) correspond to the final intensity distribution in  $WG_n$  when the light wave is initially incident from  $WG_i$ , and the final intensity distribution in  $WG_i$  when the light wave is initially incident from  $WG_n$  simultaneously, respectively. Parameter used:  $\zeta = z_f/6, \tau = z_f/10, \Omega_0 \in [1, 8]mm^{-1}$ ; Bottom frame: device length-dependent intensity of the output wave in multiple beam splitter designed by “STAP”. The value of  $\zeta$  is the same as that in Fig. 3. (c) corresponds to the case where the light wave is initially incident from  $WG_i$ ; (d) corresponds to the case where the light wave is initially incident from  $WG_m$  simultaneously. Note that the starting value of  $z$  is  $0.1mm$  and the ending value is  $10mm$ .

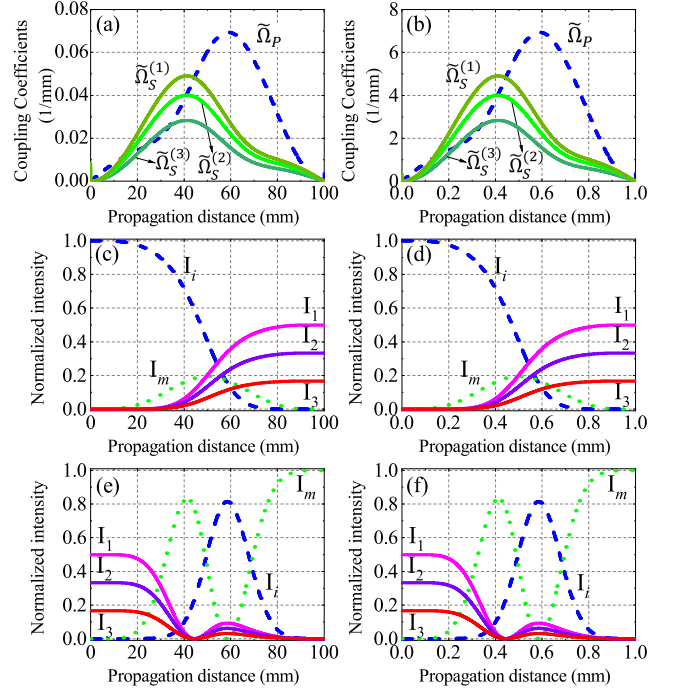


FIG. 5. (Color online) The variable multiple beam splitter designed by “STAP”. Top frame: coupling strength as a function of  $z$ ; Middle frame:  $3 : 2 : 1$  beam splitting for  $\eta_1 : \eta_2 : \eta_3 = \sqrt{3} : \sqrt{2} : 1$ ; Bottom frame: one-way optical energy transfer. Left column:  $z \in [0, 100]mm$ ; Right column:  $z \in [0, 1]mm$ . Parameter used:  $\zeta = 0.145\pi, \gamma = 0$ .

#### IV. CONCLUSIONS AND OUTLOOKS

In conclusion, a theoretical method is exhibited in this paper for multiple beam splitting by a quantum-like “STAP”. By coupling the an input and  $N$  output WGs with a mediator WG in space, efficient and robust multiple beam splitting can be achieved and the ratio of intensity can be customized arbitrarily by altering the space-dependent coupling strengths. This approach is versatile, in the sense that it can be compatible with several three-level “STAP” methods [54, 80–83]. Moreover, this novel design can significantly reduce the length of the device and can present a one-way energy transport behavior. These excellent features may have profound impacts on exploring quantum technologies for promoting advanced optical devices with simple configuration and excellent performance.

#### V. ACKNOWLEDGMENTS

I would like to thank the anonymous referees for constructive comments that are helpful for improving the quality of the work.

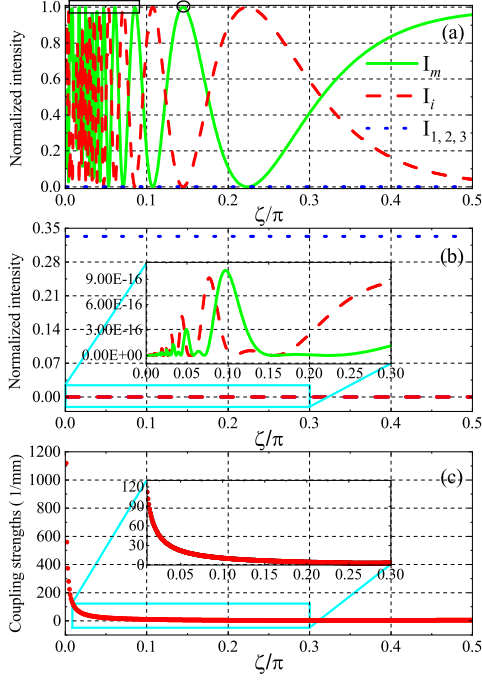


FIG. 6. (Color online) (a) The post-coupling intensity distributions as a function of  $\zeta$  for  $WG_n$  ( $n = 1, 2, 3$ ) simultaneous incidence; (b) The post-coupling intensity distributions as a function of  $\zeta$  for  $WG_i$  incidence; (c) The maximum coupling strengths as a function of  $\zeta$ . Parameter used:  $\zeta \in (0.001, 0.499)\pi$ , the step size is set to  $0.001\pi$ . All the other parameters are the same as those in Fig. 3(a).

## VI. APPENDIX

To illustrate the multiple beam splitter has a one-way wave propagation feature, it is necessary to select an appropriate value of  $\zeta$ . Notably,  $\zeta$  should  $\in (0, \frac{\pi}{2})$  as an exact zero/ $\frac{\pi}{2}$  value implies infinite/infinitesimal coupling strengths according to Eqs. (18), (19) and (25). Fig. 6(a) shows the post-coupling intensity distributions as a function of  $\zeta$  for  $WG_n$  ( $n = 1, 2, 3$ ) simultaneous incidence. The result clearly shows the output intensity of the propagation wave along  $WG_i$  and  $WG_m$  will funnel back and forth as the value of  $\zeta$  changes while that along  $WG_n$  ( $n = 1, 2, 3$ ) can be ignored. The black circle corresponds to  $\zeta = 1.45\pi$ , depicted in Fig. 3(e), which illustrates that a one-way wave propagation feature. In addition, it is easy to find additional viable values, as shown in the area in the black box, which offer a variety of options for the design of high-fidelity one-way multiple beam splitter. In contrast, the output port for incidence from  $WG_i$  is independent of the parameter  $\zeta$ , as illustrated in Fig. 6(b), which illustrates the high-fidelity multiple beam splitting from  $WG_i$  to  $WG_n$  ( $n = 1, 2, 3$ ) can always be achieved. Further calculation in Fig. 6(c) indicates that the value of  $\zeta$  is inversely proportional to the maximum coupling strengths. Therefore, by reasonably choosing the value of  $\zeta$  to determine the shape of the coupling strength, it is theoretically possible to design compact one way multiple beam splitter.

- [1] S. Longhi, *Laser & Photonics Reviews* **3**, 243 (2009).
- [2] R. Menchon-Enrich, A. Benseny, V. Ahufinger, A. D. Greentree, T. Busch, and J. Mompart, *Rep. Prog. Phys.* **79**, 074401 (2016).
- [3] I. L. Garanovich, S. Longhi, A. A. Sukhorukov, and Y. S. Kivshar, *Phys. Rep.* **518**, 1 (2012).
- [4] S. Longhi, *Phys. Rev. A* **71**, 065801 (2005).
- [5] S. Longhi, G. Della Valle, M. Ornigotti, and P. Laporta, *Phys. Rev. B* **76**, 201101(R) (2007).
- [6] F. Dreisow, A. Szameit, M. Heinrich, S. Nolte, A. Tünnermann, M. Ornigotti, and S. Longhi, *Phys. Rev. A* **79**, 055802 (2009).
- [7] B. M. Rodríguez-Lara, H. M. Moya-Cessa, and D. N. Christodoulides, *Phys. Rev. A* **89**, 013802 (2014).
- [8] W. Huang, A. A. Rangelov, and E. Kyoseva, *Phys. Rev. A* **90**, 053837 (2014).
- [9] H. Oukraou, L. Vittadello, V. Coda, C. Ciret, M. Alonzo, A. A. Rangelov, N. V. Vitanov, and G. Montemezzani, *Phys. Rev. A* **95**, 023811 (2017).
- [10] R. Alrifai, V. Coda, A. A. Rangelov, and G. Montemezzani, *Phys. Rev. A* **100**, 063841 (2019).
- [11] J. Chen, L. Deng, Y. Niu, and S. Gong, *Phys. Rev. A* **103**, 053705 (2021).
- [12] W. Song, S. Wu, Y. Chen, C. Chen, S. Gao, C. Huang, K. Qiu, S. Zhu, and T. Li, *Phys. Rev. Appl.* **17**, 014039 (2022).
- [13] G. Yang, A. V. Sergienko, and A. Ndao, *Opt. Lett.* **47**, 629 (2022).
- [14] R. Alrifai, V. Coda, T. Alhaddad, H. Taleb, A. A. Rangelov, and G. Montemezzani, *Phys. Rev. A* **107**, 013527 (2023).
- [15] R. J. C. Spreeuw, *Found. Phys.* **28**, 361 (1998).
- [16] N. V. Vitanov, A. A. Rangelov, B. W. Shore, and K. Bergmann, *Rev. Mod. Phys.* **89**, 015006 (2017).
- [17] T. Liu, A. Solntsev, A. Boes, T. Nguyen, C. Will, A. Mitchell, D. Neshev, and A. Sukhorukov, *Opt. Lett.* **41**, 5278 (2016).
- [18] K. Bergmann, N. V. Vitanov, and B. W. Shore, *J. Chem. Phys.* **142**, 170901 (2015).
- [19] H. S. Hristova, A. A. Rangelov, G. Montemezzani, and N. V. Vitanov, *Phys. Rev. A* **93**, 033802 (2016).
- [20] B. W. Shore, *Adv. Opt. Photon.* **9**, 563 (2017).
- [21] E. Paspalakis, *Opt. Commun.* **258**, 30–34 (2006).
- [22] S. Longhi, *Phys. Rev. E* **73**, 026607 (2006).
- [23] F. Dreisow, M. Ornigotti, A. Szameit, M. Heinrich, R. Keil, S. Nolte, A. Tünnermann, and S. Longhi, *Appl. Phys. Lett.* **95**, 261102 (2009).
- [24] G. Della Valle, M. Ornigotti, T. Toney Fernandez, P. Laporta, S. Longhi, A. Coppa, and V. Foglietti, *Appl. Phys. Lett.* **92**, 011106 (2008).
- [25] S.-Y. Tseng and M.-C. Wu, *J. Lightwave Technol.* **28**, 3529 (2010).

- [26] C. Ciret, V. Coda, A. A. Rangelov, D. N. Neshev, and G. Montemezzani, *Phys. Rev. A* **87**, 013806 (2013).
- [27] F.-Q. Dou, Y.-T. Wei, and Z.-M. Yan, *Nonlinear Dyn.* **111**, 12581 (2023).
- [28] H. Oukraou, V. Coda, A. A. Rangelov, and G. Montemezzani, *Phys. Rev. A* **97**, 023811 (2018).
- [29] S. Longhi, *Phys. Rev. A* **78**, 013815 (2008).
- [30] S. Longhi, *Phys. Rev. A* **79**, 023811 (2009).
- [31] C. Ciret, V. Coda, A. A. Rangelov, D. N. Neshev, and G. Montemezzani, *Opt. Lett.* **37**, 3789 (2012).
- [32] F. Dreisow, M. Ornigotti, A. Szameit, M. Heinrich, R. Keil, S. Nolte, A. Tünnermann, and S. Longhi, *Appl. Phys. Lett.* **95**, 261102 (2009).
- [33] X. Chen, R.-D. Wen, J.-L. Shi, and S.-Y. Tseng, *J. Opt.* **20**, 045804 (2018).
- [34] S. Tang, J.-L. Wu, C. Lü, J. Yao, Y. Pei, and Y. Jiang, *Appl. Phys. Lett.* **122**, 212201 (2023).
- [35] J. Leuthold and C. H. Joyner, *J. Lightwave Technol.* **19**, 700 (2001).
- [36] J. Shi, R.-Q. Ma, Z.-L. Duan, M. Liang, W. wen Zhang, and J. Dong, *Opt. Commun.* **370**, 29 (2016).
- [37] A. Hosseini, D. Kwong, C.-Y. Lin, B. S. Lee, and R. T. Chen, *IEEE J. Sel. Top. Quantum Electron.* **16**, 61 (2010).
- [38] H. S. Hristova, A. A. Rangelov, S. Guérin, and N. V. Vitanov, *Phys. Rev. A* **88**, 013808 (2013).
- [39] G. Moody, V. J. Sorger, D. J. Blumenthal, P. W. Juodawlkis, W. Loh, C. Sorace-Agaskar, A. E. Jones, K. C. Balram, J. C. F. Matthews, A. Laing, M. Davanco, L. Chang, J. E. Bowers, N. Quack, C. Galland, I. Aharonovich, M. A. Wolff, C. Schuck, N. Sinclair, M. Lončar, T. Komljenovic, D. Weld, S. Mookherjee, S. Buckley, M. Radulaski, S. Reitzenstein, B. Pingault, B. Machielse, D. Mukhopadhyay, A. Akimov, A. Zheltikov, G. S. Agarwal, K. Srinivasan, J. Lu, H. X. Tang, W. Jiang, T. P. McKenna, A. H. Safavi-Naeini, S. Steinhauer, A. W. Elshaari, V. Zwiller, P. S. Davids, N. Martinez, M. Gehl, J. Chiaverini, K. K. Mehta, J. Romero, N. B. Lingaraju, A. M. Weiner, D. Peace, R. Cernansky, M. Lobino, E. Diamanti, L. T. Vidarte, and R. M. Camacho, *J. Phys. Photonics* **4**, 012501 (2022).
- [40] S. Martínez-Garaot, E. Torrontegui, X. Chen, and J. G. Muga, *Phys. Rev. A* **89**, 053408 (2014).
- [41] B. J. Puttnam, G. Rademacher, and R. S. Luís, *Optica* **8**, 1186 (2021).
- [42] Y. Wang, Z. Hu, B. C. Sanders, and S. Kais, *Front. Phys.* **8** (2020).
- [43] E. Polino, M. Riva, M. Valeri, R. Silvestri, G. Corrielli, A. Crespi, N. Spagnolo, R. Osellame, and F. Sciarrino, *Optica* **6**, 288 (2019).
- [44] A. A. Rangelov and N. V. Vitanov, *Phys. Rev. A* **85**, 055803 (2012).
- [45] A. J. Martínez, M. I. Molina, S. K. Turitsyn, and Y. S. Kivshar, *Phys. Rev. A* **91**, 023822 (2015).
- [46] P. Vildoso, R. A. Vicencio, and J. Petrovic, *Opt. Express* **31**, 12703 (2023).
- [47] T. A. Ramadan and R. M. Osgood, *J. Lightwave Technol.* **16**, 277 (1998).
- [48] E. Torrontegui, S. Ibáñez, S. Martínez-Garaot, M. Modugno, A. del Campo, D. Guéry-Odelin, A. Ruschhaupt, X. Chen, and J. G. Muga, *Adv. At. Mol. Opt. Phys.* **62**, 117 (2013).
- [49] D. Guéry-Odelin, A. Ruschhaupt, A. Kiely, E. Torrontegui, S. Martínez-Garaot, and J. G. Muga, *Rev. Mod. Phys.* **91**, 045001 (2019).
- [50] M. Demirplak and S. A. Rice, *J. Phys. Chem. A* **107**, 9937 (2003).
- [51] M. Demirplak and S. A. Rice, *J. Chem. Phys.* **129**, 154111 (2008).
- [52] M. V. Berry, *J. Phys. A: Math. Theor.* **42**, 365303 (2009).
- [53] X. Chen, I. Lizuain, A. Ruschhaupt, D. Guéry-Odelin, and J. G. Muga, *Phys. Rev. Lett.* **105**, 123003 (2010).
- [54] X. Chen and J. G. Muga, *Phys. Rev. A* **86**, 033405 (2012).
- [55] F.-Q. Dou, Y.-T. Wei, M.-P. Han, and J.-A. Sun, *J. Opt.* **24**, 065801 (2022).
- [56] S. Tang, J.-L. Wu, C. Lü, J. Song, and Y. Jiang, *Phys. Rev. Appl.* **18**, 014038 (2022).
- [57] Y.-C. Li and X. Chen, *Phys. Rev. A* **94**, 063411 (2016).
- [58] B. T. Torosov, G. Della Valle, and S. Longhi, *Phys. Rev. A* **89**, 063412 (2014).
- [59] J.-H. Zhang and F.-Q. Dou, *New J. Phys.* **23**, 063001 (2021).
- [60] J.-H. Zhang, N. Naim, L. Deng, Y.-P. Niu, and S.-Q. Gong, *Results Phys.* **48**, 106421 (2023).
- [61] D. Stefanatos, *Phys. Rev. A* **90**, 023811 (2014).
- [62] K. Paul and A. K. Sarma, *Phys. Rev. A* **91**, 053406 (2015).
- [63] G. Della Valle, *Phys. Rev. A* **98**, 053861 (2018).
- [64] S.-Y. Tseng and X. Chen, *Opt. Lett.* **37**, 5118 (2012).
- [65] T.-Y. Lin, F.-C. Hsiao, Y.-W. Jhang, C. Hu, and S.-Y. Tseng, *Opt. Express* **20**, 24085 (2012).
- [66] S.-Y. Tseng, *Opt. Express* **21**, 21224 (2013).
- [67] X. Chen, R.-D. Wen, and S.-Y. Tseng, *Opt. Express* **24**, 18322 (2016).
- [68] S.-Y. Tseng and Y.-W. Jhang, *IEEE Photon. Technol. Lett.* **25**, 2478 (2013).
- [69] S. Martínez-Garaot, S.-Y. Tseng, and J. G. Muga, *Opt. Lett.* **39**, 2306 (2014).
- [70] C.-P. Ho and S.-Y. Tseng, *Opt. Lett.* **40**, 4831 (2015).
- [71] T.-H. Pan and S.-Y. Tseng, *Opt. Express* **23**, 10405 (2015).
- [72] F.-Q. Dou, Z.-M. Yan, X.-Q. Liu, W.-Y. Wang, and C.-C. Shu, *Optik* **210**, 164516 (2020).
- [73] G. D. Valle, G. Perozziello, and S. Longhi, *J. Opt.* **18**, 09LT03 (2016).
- [74] H.-C. Chung, S. Martínez-Garaot, X. Chen, J. G. Muga, and S.-Y. Tseng, *Europhys. Lett.* **127**, 34001 (2019).
- [75] A. K. Taras, A. Tuniz, M. A. Bajwa, V. Ng, J. M. Dawes, C. G. Poulton, and C. M. D. Sterke, *Adv. Phys.: X* **6**, 1894978 (2021).
- [76] J. Dalibard, F. Gerbier, G. Juzeliūnas, and P. Öhberg, *Rev. Mod. Phys.* **83**, 1523 (2011).
- [77] J. R. Morris and B. W. Shore, *Phys. Rev. A* **27**, 906 (1983).
- [78] A. A. Rangelov, N. V. Vitanov, and B. W. Shore, *Phys. Rev. A* **74**, 053402 (2006).
- [79] M. Saadati-Niari and M. Kiazand, *Acta Phys Pol A* **138**, 794 (2020).
- [80] S. Ibáñez, X. Chen, E. Torrontegui, J. G. Muga, and A. Ruschhaupt, *Phys. Rev. Lett.* **109**, 100403 (2012).
- [81] A. Baksic, H. Ribeiro, and A. A. Clerk, *Phys. Rev. Lett.* **116**, 230503 (2016).
- [82] X.-K. Song, Q. Ai, J. Qiu, and F.-G. Deng, *Phys. Rev. A* **93**, 052324 (2016).
- [83] J.-L. Wu, Y. Wang, J. Song, Y. Xia, S.-L. Su, and Y.-Y. Jiang, *Phys. Rev. A* **100**, 043413 (2019).



- [84] J. Zhang, L. Deng, Y. Niu, and S. Gong, (2023), [arXiv:2310.11071 \[quant-ph\]](#).
- [85] J.-L. Wu, X. Ji, and S. Zhang, *Opt. Express* **25**, 21084 (2017).
- [86] Y.-X. Shen, Y.-G. Peng, D.-G. Zhao, X.-C. Chen, J. Zhu, and X.-F. Zhu, *Phys. Rev. Lett.* **122**, 094501 (2019).
- [87] W.-P. Huang, *J. Opt. Soc. Am. A* **11**, 963 (1994).
- [88] B.-L. Weng, D.-M. Lai, and X.-D. Zhang, *Phys. Rev. A* **85**, 053801 (2012).
- [89] S. Tang, J.-L. Wu, C. Lü, J. Yao, X. Wang, J. Song, and Y. Jiang, *New J. Phys.* **25**, 033032 (2023).
- [90] B. Nedaee-Shakarab, M. Saadati-Niari, and F. Zolfagharpour, *Phys. Rev. C* **96**, 044619 (2017).
- [91] Y.-C. Li, D. Martínez-Cercós, S. Martínez-Garaot, X. Chen, and J. G. Muga, *Phys. Rev. A* **97**, 013830 (2018).
- [92] P. A. Ivanov and N. V. Vitanov, *Phys. Rev. A* **77**, 012335 (2008).
- [93] M. Amniat-Talab, M. Saadati-Niari, S. Guérin, and R. Nader-Ali, *Phys. Rev. A* **83**, 013817 (2011).
- [94] A. Yariv, *IEEE J. Quantum Electron.* **9**, 919 (1973).
- [95] R. Alrifai, V. Coda, J. Peltier, A. A. Rangelov, and G. Montemezzani, *Phys. Rev. A* **103**, 023527 (2021).